This is an *Accepted Manuscript*, which has been through the Royal Society of Chemistry peer review process and has been accepted for publication.

Accepted Manuscripts are published online shortly after acceptance, before technical editing, formatting and proof reading. Using this free service, authors can make their results available to the community, in citable form, before we publish the edited article. We will replace this *Accepted Manuscript* with the edited and formatted *Advance Article* as soon as it is available.

You can find more information about *Accepted Manuscripts* in the **Information for Authors**.

Please note that technical editing may introduce minor changes to the text and/or graphics, which may alter content. The journal's standard **Terms & Conditions** and the **Ethical guidelines** still apply. In no event shall the Royal Society of Chemistry be held responsible for any errors or omissions in this *Accepted Manuscript* or any consequences arising from the use of any information it contains.

MOF crystal growth: UV resonance Raman investigation of metal-ligand binding in solution and accelerated crystal growth methods

Thomas D. Petersen[a], Gurusamy Balakrishnan[b], Colin L. Weeks[a],*

[a]Department of Chemistry and Biochemistry, University of Northern Iowa, Cedar Falls, IA, 50614, USA

[b]Department of Chemistry, University of Washington, Seattle, WA, 98195, USA

Address for correspondence:

Colin L. Weeks

Department of Chemistry and Biochemistry

University of Northern Iowa

Cedar Falls, IA, 50614, USA

Email: colin.weeks@uni.edu,

Phone: +1 319-273-2805,

Fax: +1 319-273-7127

Table of Contents Entry
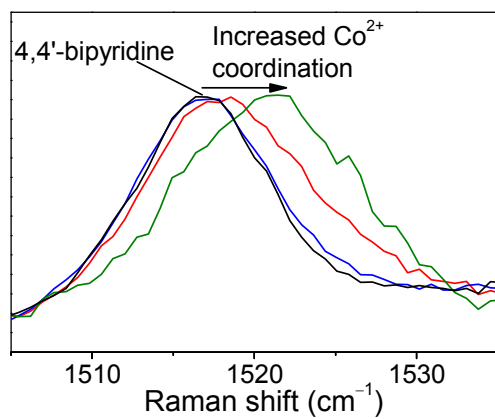
Resonance Raman spectroscopy can detect metal-ligand binding in solution during the

formation of MOF crystals.

Abstract

Determining the mechanism of metal-organic framework (MOF) crystal growth is important for the development of more efficient and reliable synthetic methods. Resonance Raman spectroscopy has been used for the first time to detect interactions in solution between metal ions and bridging ligands as MOFs form. UV excitation (229 nm) produced strong resonance enhancement of 4,4'-bipyridine (bpy) vibrational bands and showed that soluble Co^{2+}-bpy species formed in solution prior to the growth of MOF crystals from bpy and $Co(NO_3)_2$. The results of the Raman experiments informed the development of faster methods for synthesizing $[Co_2(bpy)_3(NO_3)_4]_n$ 2D bilayer and $[Co(bpy)(NO_3)_2(H_2O)_2]_n$ 1D chain MOFs.

Introduction

Metal-organic frameworks (MOFs) are of considerable interest as control of their structure can produce properties such as magnetism,[1-3] catalytic activity[4-6] and selective guest sorption.[7-9] The structure of MOFs depends on numerous factors including the identity of the metal ion and organic bridging ligand, the solvent,[10-12] the counterion[13, 14] and pH.[15, 16] Another challenge is that the common methods for making MOFs, solvothermal synthesis and slow diffusion, often take several days to several months to produce crystals. Knowing the mechanisms by which MOFs form will help efforts to control MOF structure and to develop more efficient synthetic methods. Most knowledge of the factors affecting MOF crystal growth has been obtained by determining the crystal structures of MOFs produced by different synthetic conditions. However, a few studies have directly probed the mechanism of MOF formation.

A key question in MOF formation is: Do the metal ion and bridging ligand bind in solution to form a complex that adds to the growing crystal or do they add separately to the surface of the crystal as it grows? ^{27}Al NMR spectroscopy showed that both monomeric and dimeric Al species were present in solution during the formation of Al-trimesate MOFs.[17] ESI-MS measurements identified both monomeric Mg^{2+} and dimeric secondary building units (SBUs) in solutions used to grow MOFs from Mg^{2+} and (+)-camphoric acid.[18] An ESI-MS investigation of the changes in solution speciation during the formation of ZIF-8 crystals provided strong evidence that a tetranuclear or related oligomeric Zn species in which the Zn^{2+} were bridged by 2-methylimidazolate ligands played an important role in crystal nucleation.[19] An EXAFS study of MIL-89 formation showed that the SBUs remained intact during the hydrothermal crystallization

process.[20] In contrast, AFM studies of MOF-5 and HKUST-1 found that the crystals grew predominately by direct addition of individual ligands and simple solvated M^{2+} or M^{2+}-ligand ions, rather than by the addition of multinuclear SBUs.[21, 22] However, another study on HKUST-1, using surface plasmon resonance, found that a Cu^{2+} precursor salt that favored SBU formation in solution increased the MOF growth rate.[23] These studies indicate that the mechanism of crystal growth differs for various MOFs, and in some cases the data is conflicting. Hence, the crystal growth mechanism needs to be determined for each MOF of interest.

In this paper we report that resonance Raman (RR) spectroscopy can be used to detect the interaction between a metal ion and a bridging ligand in solution during the growth of MOF crystals. While Raman spectroscopy (usually non-resonant) has been used to characterize solid MOFs[24, 25] and to investigate the interaction of guest molecules with the framework of porous MOFs[26-28] this is the first time that it has been used to observe species present in solution during MOF crystal growth.

MOFs prepared from cobalt(II) nitrate and 4,4'-bipyridine (bpy) were chosen for study because a large number of MOFs have been synthesized using bpy[10-12, 29, 30] and related pyridyl-based bridging ligands.[26, 31] The $\pi \rightarrow \pi^*$ electronic transition of bpy in the UV made it a good candidate for obtaining strong RR signals with UV excitation. Slow diffusion reactions in ethanol produce a $[Co_2(bpy)_3(NO_3)_4]_n$ 2D bilayer framework (Figure 1)[10] and in ethanol/water a $[Co(bpy)(NO_3)_2(H_2O)_2]_n$ 1D chain structure (Figure 2)[30] is formed.
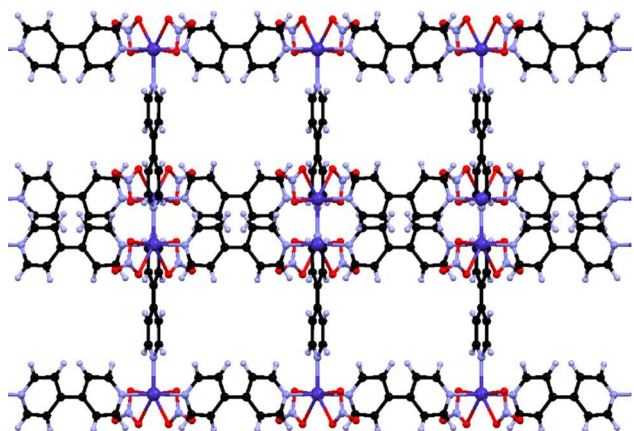
Figure 1. Structure of the [Co$_2$(bpy)$_3$(NO$_3$)$_4$]$_n$ 2D bilayer framework[10] produced from CCDC-

100832 showing the interpenetration of two bilayers and the coordination geometry around

the Co.[10]
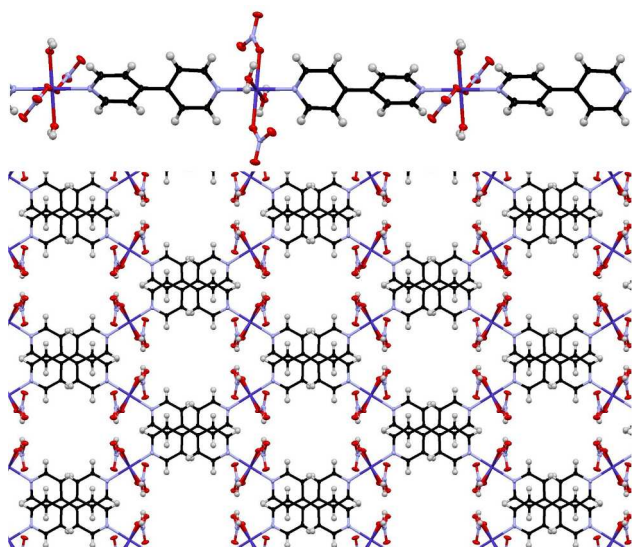
Figure 2. Structure of a single [Co(bpy)(H$_2$O)$_2$(NO$_3$)$_2$]$_n$ 1D chain and the packing of the 1D chains

in the crystal.[30]

Experimental

Materials

Cobalt(II) nitrate hexahydrate (Alfa Aesar, 97.7%) was dried over anhydrous calcium sulfate prior to use. 4,4'-bipyridine (bpy) (Acros, 98%) and absolute ethanol (Acros, 99.8%; Pharmaco Aaper 99.5%; or Calbiochem, Omnipure 200 proof) were used as received.

Slow Diffusion Crystal Growth Reactions

The slow diffusion methods used to grow the MOF crystals were based on previously described procedures.[10, 30, 32] Diffusion reactions were carried out in 12 mL vials (Supplementary Data, Figure S1).

$[Co_2(bpy)_3(NO_3)_4]_n$ 2D Bilayer Framework

Cobalt(II) nitrate hexahydrate (0.050 g) was dissolved in ethanol (1.0 mL) and a layer of absolute ethanol (5.0 mL) was added. Finally a solution of bpy (0.040 g) in ethanol (4.0 mL) was layered on top. Solution samples were removed from the vial and used to measure the RR and UV-vis spectra.

$[Co(bpy)(H_2O)_2(NO_3)_2]_n$ 1D Chains

Cobalt(II) nitrate hexahydrate (0.050 g) was dissolved in ethanol (1.0 mL) and 0.5 mL of water was added to the solution. A layer of absolute ethanol (5.0 mL) was added and then a solution of bpy (0.040 g) in ethanol (4.0 mL) was layered on top. Solution samples were removed from the vial and used to measure the RR and UV-vis spectra.

Direct Mixing Crystal Growth Reactions

[Co$_2$(bpy)$_3$(NO$_3$)$_4$]$_n$ 2D Bilayer Framework

Final concentration 1.0 mM Co(NO$_3$)$_2$ and 1.5 mM bpy: Cobalt(II) nitrate hexahydrate (0.119 g) was dissolved in ethanol (200.0 mL) and mixed with a solution of bpy (0.094 g) in ethanol (200.0 mL). No colour change was observed when the solutions were mixed and no crystals formed.

Final concentration 2.0 mM Co(NO$_3$)$_2$ and 3.0 mM bpy: Cobalt(II) nitrate hexahydrate (0.058 g) was dissolved in ethanol (50.0 mL) and mixed with a solution of bpy (0.049 g) in ethanol (50.0 mL). No colour change was observed when the solutions were mixed. After 1 day trace amounts of red crystals had formed, but the amount was insufficient for characterization.

Final concentration 5.0 mM Co(NO$_3$)$_2$ and 7.5 mM bpy: Cobalt(II) nitrate hexahydrate (0.146 g) was dissolved in ethanol (50.0 mL) and mixed with a solution of bpy (0.117 g) in ethanol (50.0 mL). The pink Co(NO$_3$)$_2$ solution became slightly orange in hue when the solutions were mixed, but no crystals formed immediately. 20 min after mixing the orange tint in the solution was more pronounced and a tiny amount of red crystals had formed. After 1 day the product was collected by vacuum filtration on a sintered glass frit. The crystals were dried overnight at 90 °C prior to elemental analysis. Yield 0.152 g (73%). Found: C, 42.7%; H, 2.8%; N, 15.8%. [Co$_2$(bpy)$_3$(NO$_3$)$_4$] C$_{30}$H$_{24}$N$_{10}$Co$_2$O$_{12}$ requires C, 43.2%; H, 2.9%; N, 16.8%.

Final concentration 10 mM Co(NO$_3$)$_2$ and 15 mM bpy: Cobalt(II) nitrate hexahydrate (0.292 g) was dissolved in ethanol (50.0 mL) and mixed with a solution of bpy (0.236 g) in ethanol (50.0 mL). The pink Co(NO$_3$)$_2$ solution became slightly orange in hue when the solutions were mixed, but no crystals formed immediately. 10 min after mixing the orange tint in the

solution was slightly more noticeable and a tiny amount of red crystals had formed. After 1 day

the product was collected by vacuum filtration on a sintered glass frit. The solvated crystals

were used to record the PXRD pattern. The crystals were dried overnight at 90 °C prior to

elemental analysis. Yield 0.381 g (91%). Found: C, 42.6%; H, 2.8%; N, 15.9%. $C_{30}H_{24}N_{10}Co_2O_{12}$

requires C, 43.2%; H, 2.9%; N, 16.8%.

Final concentration 38 mM $Co(NO_3)_2$ and 57 mM bpy: Cobalt(II) nitrate hexahydrate

(0.201 g) was dissolved in ethanol (4.0 mL) and mixed with a solution of bpy (0.161 g) in ethanol

(14.0 mL). A very fine powdery pink precipitate formed immediately. The product was collected

by vacuum filtration on a sintered glass frit. The solvated crystals were used to record the PXRD

pattern. The crystals were dried overnight at 90 °C prior to elemental analysis. Yield 0.267 g

(93%). Found: C, 41.8%; H, 2.8%; N, 15.3%. $C_{30}H_{24}N_{10}Co_2O_{12}$ requires C, 43.2%; H, 2.9%; N,

16.8%.

[Co(bpy)(H_2O)_2(NO_3)_2]_n 1D Chains

Final concentration 19 mM $Co(NO_3)_2$ and 19 mM bpy: Cobalt(II) nitrate hexahydrate

(0.100 g) was dissolved in ethanol (5.0 mL) and then 1.0 mL of water was added, forming a pale

pink solution. The $Co(NO_3)_2$ solution was mixed with a solution of bpy (0.054 g) in ethanol (12.0

mL) and the colour changed to pink-orange. No crystals formed when the solutions were mixed.

After 1 day small orange rectangular prism crystals formed, and they were collected by vacuum

filtration on a sintered glass frit. Yield 0.102 g (72%). Found: C, 32.8%; H, 3.75%; N, 13.1%.

$[Co(bpy)(H_2O)_2(NO_3)_2] \cdot 0.5H_2O \cdot 0.5CH_3CH_2OH$ $C_{11}H_{16}N_4CoO_9$ requires: C, 32.4%; H, 4.0%; N,

13.8%.

Characterization

Raman Spectroscopy

Resonance Raman spectra were obtained at 220 nm and 229 nm. Excitation pulses at 220 nm and 229 nm (1.0 μJ/pulse) were obtained by frequency quadrupling the output of a Ti: sapphire laser, which was pumped (527 nm, ≈10mJ/pulse, 70 ns, 1 kHz) by an intracavity frequency-doubled Nd: YLF laser (GM30, Photonics International, Inc.).[33] The spectra of $Co(NO_3)_2$ and 4,4'-bipyridine in ethanol were measured using solutions sealed in 5 mm quartz NMR tubes, which contained a micro magnetic stir bar and were spun to ensure mixing of the solution. The scattered light was collected at a 135° backscattering geometry and focused onto a 1.26 m spectrograph (Spex 1269, 3600 grooves/mm grating) equipped with a liquid nitrogen-cooled CCD camera (Roper Scientific). The laser power at the sample was ~1mW. Raman spectra were measured using 10×30 s collections. The individual 30 s spectra were checked for changes over the course of the data collection before averaging them together. Calibration and peak-fitting analysis of the spectra were carried out using GRAMS AI software (Thermo Electron Corp.). Acetone was used as the calibration standard.

The RR spectra of ethanol solutions containing 1 mM bpy and 1-9 mM of $Co(NO_3)_2$ were recorded to determine whether bands in the bpy spectrum were sensitive to the binding of bpy to Co^{2+} in solution. The low bpy concentration prevented the formation of precipitates during the measurement of the Raman spectra.

UV-vis Spectroscopy

UV-vis spectra were recorded from 400-600 nm on a Thermo Scientific Evolution 300 spectrophotometer. The solutions were placed in a 1.00 cm quartz cell. Solution samples were

taken from the slow diffusion crystal growth reactions and immediately after combining

$Co(NO_3)_2$ and bpy solutions in the direct mixing MOF syntheses. Spectra were also recorded of

solutions with 5.0 mM $Co(NO_3)_2$ and 1.0-10.0 mM bpy in ethanol immediately after mixing.

Powder X-ray Diffraction

Powder X-ray diffraction (PXRD) patterns of crystalline samples were measured using Cu

Kα radiation (λ = 1.54059 Å) on a Rigaku Miniflex II diffractometer. Crystal samples were ground

to a powder and loaded onto a low background silicon sample holder. Data was collected from

5° to 50° or 55° in 2θ using continuous sampling with ω= 0.050°, scan rate= 2° min^{-1}, V = 20 kV,

and I = 15 mA.

Results and Discussion

The Raman spectrum of a 1.0 mM solution of bpy in ethanol showed strong resonance

enhancement of the bpy vibrational bands using 229 nm excitation (Supplementary Data, Figure

S2). The signal-to-noise ratio of the bpy bands was high, and they were similar in intensity to the

ethanol bands, even though the concentration of bpy was four orders of magnitude lower. The

contribution of the ethanol bands could be subtracted from the spectra using the isolated 890

cm^{-1} ethanol band to normalize the intensities (Supplementary Data, Figure S3). Peak fitting of

the spectra showed that subtracting the ethanol bands from the spectrum did not alter the

position or shape of the bpy bands (Supplementary Data, Table S1), so spectra are shown after

ethanol band subtraction. Raman spectra of bpy solutions were also collected using 220 nm

excitation, but the signal to noise ratio was lower (data not shown), so all subsequent

experiments used 229 nm excitation.

The RR spectra of solutions containing 1 mM bpy and 1-9 mM of $Co(NO_3)_2$ in ethanol showed that the binding of bpy to Co^{2+} in solution could be detected (Figure 3). The A_g δCH mode of bpy was blue-shifted by 3 cm^{-1} when 9 mM of Co^{2+} was added and the bpy A_g ν_{ring} mode at 1517 cm^{-1} was blue-shifted by 5 cm^{-1} when 9 mM of Co^{2+} was added. The changes in the positions of these two bands were Co^{2+} concentration dependent. An IR and Raman spectroscopic study of solid samples of bpy, $Cd(bpy)Cl_2$, $Zn(bpy)Cl_2$ and $Cu(bpy)Cl_2$ by Topaçli and Akyüz showed that the the bpy A_g ν_{ring} mode at 1514 cm^{-1} was blue-shifted by 6-9 cm^{-1} when the bpy was coordinated to M^{2+} ions and the A_g δCH mode at 1230 cm^{-1} was blue-shifted by 5-8 cm^{-1} when the bpy was coordinated to M^{2+} ions.[34] The Raman spectra of crystalline Fe(II) and Zn(II) coordination polymers in which the M^{2+} ions were bridged by bpy to form a 1D chain had a ν_{ring} mode that was blue-shifted by 4-6 cm^{-1} compared to the bpy ν_{ring} mode at 1513 cm^{-1}.[35] The Co^{2+} concentration dependence of the shift in position of these bpy bands and the evidence that these vibrational modes are blue-shifted when bpy coordinates to transition metal cations clearly demonstrate that the changes observed in the bpy Raman spectrum when Co^{2+} was added were due to the coordination of bpy to Co^{2+}. There were additional changes in the bpy spectrum due to Co^{2+} coordination. As the concentration of Co^{2+} increased the intensity of the 1007 cm^{-1} band decreased. The relative intensity of the 1611 cm^{-1} and 1623 cm^{-1} bpy bands was also a good marker of Co^{2+} binding to bpy. The 1611 cm^{-1} band was slightly more intense in the bpy spectrum, but the addition of Co^{2+} caused the intensity of the 1611 cm^{-1} band to decrease and the intensity of the 1623 cm^{-1} band to increase systematically as the Co^{2+} concentration increased. The Co^{2+} concentration dependence of the 1611 cm^{-1}/1623 cm^{-1} band intensity ratio showed that these changes in the bpy Raman spectra were due to the

coordination of the Co^{2+} to the bpy. This shows that some of the resonance enhanced bpy bands were sensitive to metal ion coordination, and hence UVRR spectroscopy can be used to detect the interaction of Co^{2+} and bpy in dilute solutions such as those used in MOF crystal growth.
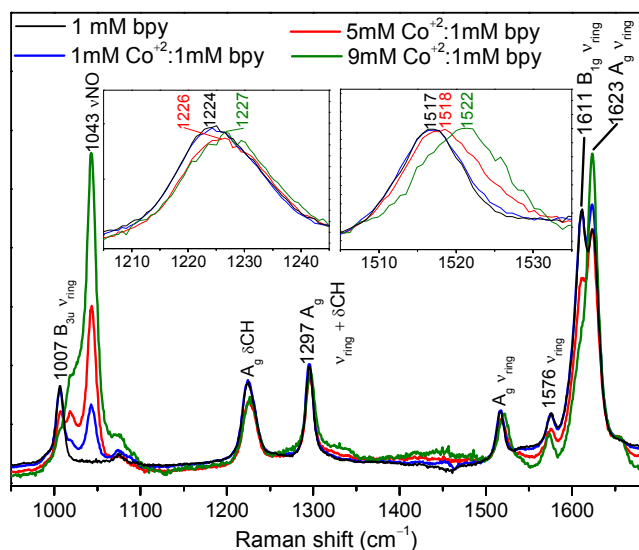
Figure 3. Raman spectra of 1 mM bpy with 1-9 mM $Co(NO_3)_2$ in ethanol and vibrational band assignment[34, 36]. Ethanol spectrum subtracted, λ_{ex} = 229 nm.

Since RR spectroscopy could detect Co^{2+}-bpy binding in solution, spectra were recorded of solution from the region of the vial where 2D bilayer crystals were forming in the slow diffusion reaction and of solutions from higher levels in the vial with no crystals had yet formed. After 1 day of diffusion substantial amounts of 2D bilayer crystals had formed on the sides of the vial near the bottom. The RR spectra (Figure 4) showed that the two solution samples from the top part of the vial contained mostly bpy as the 1043 cm^{-1} band due to the νNO band of the nitrate anion was very small and there was little change in the bpy bands. In the spectrum of the sample taken 10 mm above the point at which the crystals were growing the A_g δCH mode

and the A_g ν_{ring} mode at 1518 cm^{-1} of bpy were blue-shifted by 1 cm^{-1}, and the intensity of the 1623 cm^{-1} band was moderately greater than the intensity of the 1611 cm^{-1} band. This indicated that a small proportion of bpy was coordinated to Co^{2+}. The sample of solution taken from the region in which the 2D bilayer crystals were growing showed large changes in the bpy bands. The A_g δCH mode was blue-shifted by 4 cm^{-1}, and the A_g ν_{ring} mode had blue-shifted by 6 cm^{-1} to 1523 cm^{-1}. The shifts in the positions of these bands in the solution taken from the crystal growth region are slightly larger than the shifts observed at the maximum Co:bpy ratio of 9:1 in Figure 3. The 6 cm^{-1} shift in the A_g ν_{ring} mode in now within the range of the 6-9 cm^{-1} and 4-6 cm^{-1} shifts observed when bpy coordinated to two metal cations[34, 35] and the 4 cm^{-1} shift in the A_g δCH mode is just a bit smaller than the 5-8 cm^{-1} shift observed when bpy coordinated to two metal cations.[34] This indicates that it is possible that an appreciable portion of the bpy in the solution taken from the crystal growth region is coordinated to two Co^{2+} ions. The intensity of the 1623 cm^{-1} band dramatically increased, and it was much greater in intensity than the 1611 cm^{-1} band. This intensity change also shows that there were substantial amounts of bpy bound to Co^{2+} in the solution around the growing crystals. It should be noted that a much larger proportion of bpy in solution had Co^{2+} bound to it in the region where crystals were growing than in the solution from 10 mm higher up the vial where no crystals had formed. This indicated that soluble Co^{2+}-bpy species were possibly acting as intermediates in the formation of the 2D bilayer crystals.
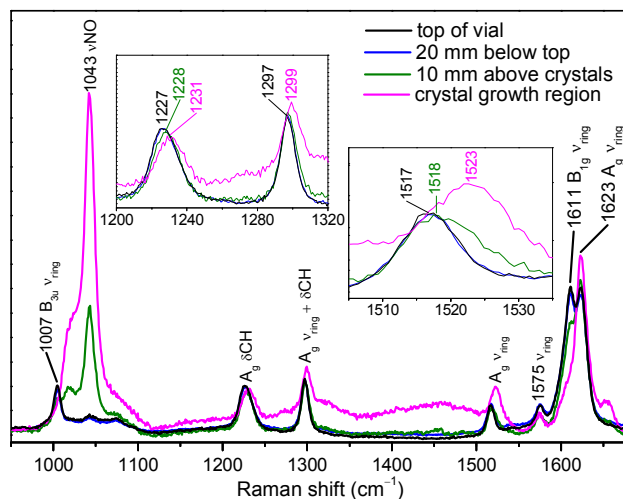
Figure 4. Raman spectra of solution samples from different points in the vial after diffusing bpy and Co(NO$_3$)$_2$ in ethanol for 1 day to form 2D bilayer crystals. Ethanol spectrum subtracted, λ_{ex} = 229 nm.

The growth of 1D chain crystals by slow diffusion takes days to weeks[30] so no crystals were present when solution samples were used to record the RR spectra after diffusing for 1 day. The RR spectrum of the solution taken from the middle of the vial showed that there was substantial binding of bpy to Co^{2+} (Figure 5). The A_g δCH mode was blue-shifted by 4 cm^{-1}, and the A_g ν_{ring} mode had blue-shifted by 4 cm^{-1} to 1521 cm^{-1}. The intensity of the 1007 cm^{-1} band had decreased and the 1623 cm^{-1} band was substantially greater in intensity than the 1611 cm^{-1} band. The RR data indicated that substantial amounts of soluble Co^{2+}-bpy species formed prior to 1D chain MOF crystal formation.
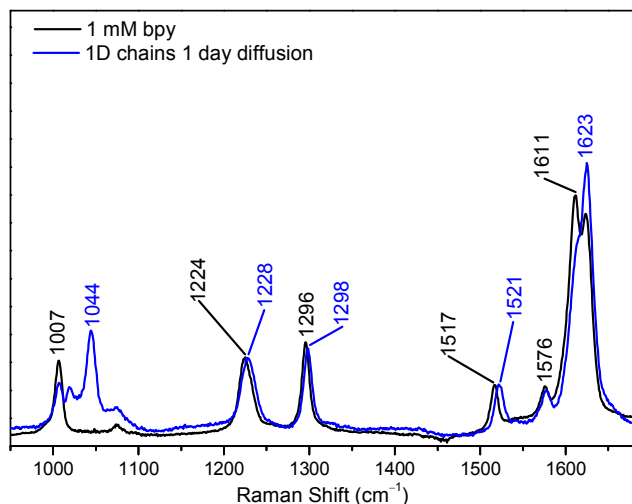
Figure 5. Raman spectra of bpy and a solution sample taken from a 1D chain slow diffusion reaction. The solution was taken from the middle of the vial after diffusing bpy and $Co(NO_3)_2$ in ethanol/water for 1 day. Ethanol spectrum subtracted, λ_{ex} = 229 nm.

The UV-vis absorption spectra of the solutions from the crystal growth region of the slow diffusion reactions confirmed the presence of soluble Co^{2+}-bpy species. For the 2D bilayer the λ_{max} of the Co $d{\rightarrow}d$ transition was at 517 nm, a blue-shift of 4 nm compared to $Co(NO_3)_2$ in ethanol (Supplementary Data, Figure S5). A 6 nm blue shift of the λ_{max} was observed for the 1D chain MOF crystal growth solution (Supplementary Data, Figure S6). The shift of the Co $d{\rightarrow}d$. transition to higher energy in both experiments showed that bpy was binding to the Co^{2+}, as pyridyl groups are stronger field ligands than ethanol, water or nitrate. The other ligands in the soluble Co^{2+}-bpy species formed during the growth of the 2D bilayer crystals must be mostly water or ethanol and not nitrato because the λ_{max} of 517 nm of the solution from the crystal growth region is at a shorter wavelength than the λ_{max} of 527 nm found for $[Co(pyridine)_3(NO_3)_2]$ in chloroform solution.[37] Pyridine and bpy are very similar in ligand field

strength and it is unlikely that the number of bpy (the strongest field ligand present in these solutions) coordinated per Co would exceed the three bpy per Co found in the final 2D bilayer structure.

The UV-vis and RR spectra provide complementary information. The shift of the *d-d* transition in the UV-vis spectra provides a measure of the relative number of pyridyl groups coordinated to each Co^{2+}, while the bpy bands in the RR spectra provide a measure of the relative proportion of bpy that are coordinated to Co^{2+}. The RR spectra of bpy with various ratios of Co^{2+} (Figure 3) showed that Co:bpy ratios of 5:1-9:1, which far exceeded the Co:bpy ratios present in the 2D bilayer MOF product grown in ethanol, were required to have a substantial proportion of the bpy in solution bound to Co^{2+}. The shift in the bpy A_g δCH and A_g ν_{ring} band positions and changes in 1611 cm^{-1}/1623 cm^{-1} band intensity ratio in the RR spectrum from the crystal growth region for the bilayer crystals (Figure 4) showed that the Co:bpy ratio in the solution around the growing 2D bilayer crystals was at least 9:1 and quite possibly was higher.

The initiation of 2D bilayer MOF crystal growth near the bottom of the vial could be due to a couple different reasons. One possible explanation is that the soluble Co^{2+}-bpy species detected near the bottom of the vial are intermediates in the formation of the MOF crystals and substantial amounts of the intermediate are required for crystal growth to occur. The other possible explanation is that the total concentrations of Co^{2+} and bpy were simply not large enough higher up the vial for precipitation of the MOF product to occur. It is not possible to conclusively distinguish between these two possibilities based on the RR and UV-vis data, because it is difficult to determine the identity of the soluble Co^{2+}-bpy species. The progressive

changes in the RR bands of bpy as the Co:bpy ratio was varied from 1:1 to 9:1 (Figure 3) and the continual shift in the λ_{max} of the Co $d{\rightarrow}d$. transition as the Co:bpy ratio was varied from 5:1 to 1:2 (Supplementary Data, Figure S7) suggested that more than one Co^{2+}-bpy species was present in solution. This was probably also true of the solutions in the crystal growth regions of the slow diffusion reaction vials. Though it was not possible to identify a specific Co^{2+}-bpy solution species as the precursor to MOF crystal growth the RR spectroscopy provided the important insight that Co^{2+} binds to a substantial proportion of the bpy in solution around the growing crystals of the 2D bilayer and 1D chain MOFs.

Though it was not possible to identify a specific soluble Co^{2+}-bpy species as the MOF precursor, the identification of such species by RR spectroscopy raised the possibility that controlled formation of soluble Co^{2+}-bpy species could be used to develop faster methods of growing 2D bilayer and 1D chain MOF crystals than the slow diffusion procedures usually used to produce these crystals. An observation made during the RR experiments also contributed to the genesis of this idea. The solution from the crystal growth region of the 2D bilayer slow diffusion reaction had some tiny crystals in it at the end of collecting the RR spectrum. The crystals formed outside the zone irradiated by the laser, so they did not contribute to the Raman spectrum. However, this observation indicated that forming the same soluble Co^{2+}-bpy species as were present in the crystal growth region of the slow diffusion reaction might lead to a method for producing 2D bilayer crystals by direct mixing at room temperature. It indicated that it should be possible to find conditions under which Co^{2+} and bpy were present in sufficient concentrations to form MOF crystals, but where they would form soluble species when initially combined, rather than immediately precipitating as an impure mix of products.

18

When the metal ions and bridging ligand(s) that form a MOF are directly mixed it is usually necessary to use solvothermal methods, heating to temperatures above the usual boiling point of the solvent then very gradually cooling the sample, to obtain high quality crystalline products. This process requires large amounts of energy and is slow, it takes several days to heat up and gradually cool down the sample. Direct mixing of the metal ions and bridging ligand(s) at room temperature would greatly lower energy requirements and is potentially substantially quicker, but it is rarely used to prepare MOFs due to the formation of mixed products or amorphous material.

The results from the RR spectra were used to guide the choice of bpy and $Co(NO_3)_2$ concentrations for direct mixing experiments. As no crystals formed in the 1 mM bpy + 1-9 mM $Co(NO_3)_2$ solutions in ethanol used to determine the effect of Co^{2+} binding on the RR spectrum of bpy, the tests mostly used $Co(NO_3)_2$ concentrations from 1-10 mM, but with larger proportions of bpy than in the solutions for RR spectroscopy so that the Co:bpy ratio matched the 2:3 ratio found in the 2D bilayer crystals. A 38 mM $Co(NO_3)_2$ and 57 mM bpy concentration mixture was also tested in direct mixing experiments because it used the same concentrations of $Co(NO_3)_2$, bpy and ethanol as a typical diffusion reaction without the intermediate layer of pure ethanol that prevents direct mixing.[30]

The mixture with $[Co^{2+}]$ = 1.0 mM after mixing did not produce any crystals, and in the mixture with $[Co^{2+}]$ = 2.0 mM trace amounts of red crystals formed 1 day after mixing. When the $[Co^{2+}]$ was in the 5-10 mM range the color changed from the pink to pink-orange when the bpy solution was added (Figure 6). With $[Co^{2+}]$ = 5-10 mM tiny red crystals would usually start to grow a few minutes after mixing. The crystals formed by direct mixing with $[Co^{2+}]$ = 5-10 mM

were much smaller than the crystals grown by slow diffusion, but they were clearly crystalline (Figure 6c). In some experiments with $[Co^{2+}]$ = 5-10 mM no crystals had formed 30 min after mixing. In these cases the flask was gently shaken for 1-2 s, whereupon a large amount of tiny red crystals rapidly formed. The very rapid formation of large amounts of 2D bilayer crystals upon disturbance of the solution is most likely due to the solution being saturated with a soluble Co^{2+}-bpy MOF precursor species and rapid crystal growth occurred when nucleation of the MOF crystals was triggered by shaking the flask. This is a strong indication that soluble Co^{2+}-bpy species do play a role as intermediates in the growth of the 2D bilayer crystals. Though it appears from the RR and UV-vis spectra that more than one soluble Co^{2+}-bpy species can form in ethanol solution, the almost instantaneous formation of crystals when the flask was shaken after standing for 30 min indicates that a major soluble Co^{2+}-bpy species was probably an intermediate in MOF formation. The UV-vis spectrum of the 10 mM $Co(NO_3)_2$ + 15 mM bpy solution immediately after mixing was identical to the spectrum of the solution from the crystal growth region of the slow diffusion reaction (Supplementary Data, Figure S5). This showed that the same mix of soluble Co^{2+}-bpy species formed in the slow diffusion and direct mixing reactions, which is consistent with soluble species acting as precursors to MOF crystal growth. When the $[Co^{2+}]$ was 38 mM and [bpy] was 57 mM, equivalent to the concentrations used in a slow diffusion reaction,[30] a fine pink precipitate formed immediately upon mixing.
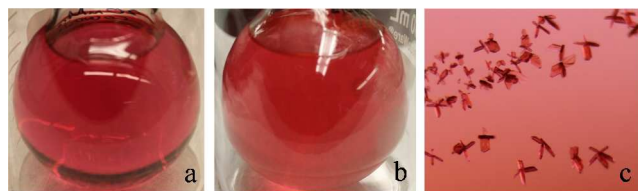
Figure 6. a) 20 mM $Co(NO_3)_2$ in ethanol b) 10 mM $Co(NO_3)_2$ and 15 mM bpy in ethanol 1 min

after mixing c) 2D bilayer crystals formed by direct mixing of 10 mM $Co(NO_3)_2$. + 15 mM bpy in

ethanol.

The PXRD patterns showed that the crystals grown by direct mixing of $Co(NO_3)_2$ and bpy

solutions were the 2D bilayer structure (Figure 7). There was excellent agreement in the peak

positions to the 2D bilayer crystals grown by slow diffusion, and no additional crystalline phases

were detected when the PXRD pattern was compared to the pattern calculated from the

reported SCXRD structure (Supplementary Data, Figure S9 and Table S2). The peaks were

broader in the patterns of the direct mixing samples, and the peak width increased with

increasing concentration of the $Co(NO_3)_2$ and bpy. The peak broadening was probably due to

increased mosaicity, and in the fine powder produced by the reaction of 38 mM $Co(NO_3)_2$ + 57

mM bpy small particle size may have also contributed. Elemental analysis showed that the

product of the reaction of 38 mM $Co(NO_3)_2$ + 57 mM bpy was not pure, the C and N content

were 1.4-1.5% lower than the calculated values. The high Co^{2+} and bpy concentrations led to the

precipitation of solids with other structures. This showed that controlling the concentration to

ensure selective precipitation was important for MOF purity. Thus the best concentrations for

growing 2D bilayer crystals was 10 mM $Co(NO_3)_2$ + 15 mM bpy as this produced pure crystals in

91% yield. Thus direct mixing of these concentrations of $Co(NO_3)_2$ and bpy solutions avoids the

immediate precipitation of mixtures of products while still producing large amounts of pure 2D

bilayer crystals in good yield. Not only are the 2D bilayer crystals produced more rapidly than in

the slow diffusion crystal growth method previously used, but production is much easier to

scale up as the laborious process of slowly layering three solutions into multiple vials is no

longer necessary.
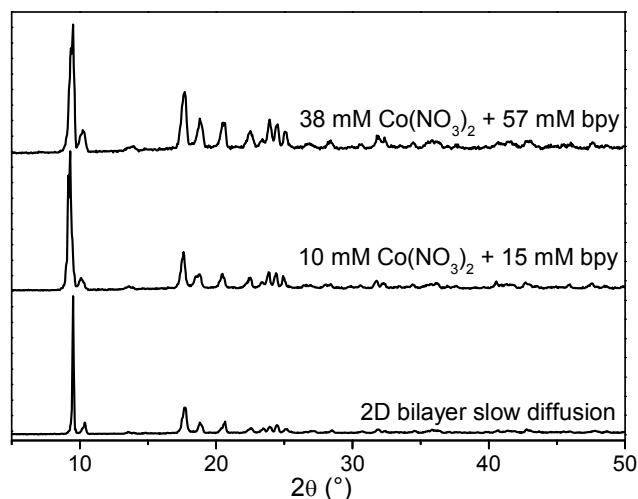
Figure 7. PXRD patterns of 2D bilayer crystals grown by slow diffusion and by direct mixing of

ethanol solutions of $Co(NO_3)_2$ and bpy.

The RR evidence for soluble Co^{2+}-bpy species present in solution prior to 1D chain crystal

formation indicated that the crystals of this MOF could also be prepared by direct mixing of

$Co(NO_3)_2$ and bpy solutions. An ethanol/water solution that was 19 mM $Co(NO_3)_2$ + 19 mM bpy

was prepared by direct mixing and small orange crystals formed overnight. The aqua ligands

bound to the Co^{2+} in the ethanol/water solution (Supplementary Data, Figure S6) meant that

higher concentrations of $Co(NO_3)_2$ and bpy could be used than for the 2D bilayer without an

impure product immediately precipitating. The PXRD pattern showed that the product of the

direct mixing reaction matched the PXRD pattern of the 1D chain crystals grown by slow

diffusion (Figure 8) and was in good agreement with the PXRD pattern calculated from the

SCXRD data (Supplementary Data, Figure S10 and Table S3). The similar peak widths in the PXRD

pattern showed that the crystals produced by direct mixing were comparable in quality to those

grown by slow diffusion. The formation of the 1D chain crystals overnight in the direct mixing

reaction was a great improvement on the days to weeks required by the slow diffusion

method.[30]
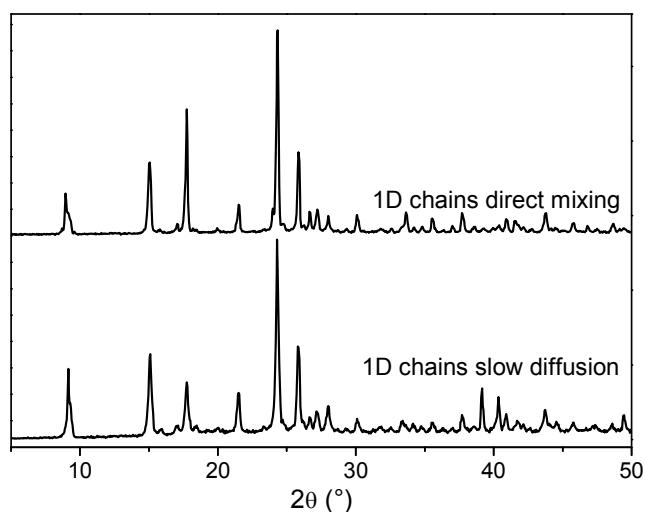
Figure 8. PXRD patterns of 1D chain crystals grown by slow diffusion and by direct mixing of

ethanol/water solutions of $Co(NO_3)_2$ and bpy.

Conclusions

The determination from the RR spectra that substantial amounts of soluble Co^{2+}-bpy

species formed in solution prior to the formation of the 2D bilayer and 1D chain MOF crystals

led to the development of much faster direct mixing methods for producing these MOFs. RR

spectroscopy can now be added to the methods that are useful for elucidating the mechanism

of MOF crystal growth. The very strong resonance-enhancement of bpy bands that are sensitive

to metal ion coordination means that it is a powerful new approach for studying the interaction of the metal ions and bpy in solution as MOF crystals form. While only systems containing bpy were investigated in this study it is likely that this technique could be successfully applied to MOFs containing the numerous other pyridyl-based bridging ligands that have been reported. Similar metal-binding sensitive pyridyl ring vibrational modes should be resonance enhanced by excitation wavelengths coinciding with the $\pi \rightarrow \pi^*$ electronic transition of these ligands.

Supplementary Data

Schematic diagram of slow diffusion crystal growth set up. Raman spectra of bpy and vibrational mode assignments. UV-vis spectra of crystal growth solutions. 1D chain crystal growth photo. Simulated PXRD patterns.

Acknowledgements

References

1.	S. R. Batten, P. Jensen, C. J. Kepert, M. Kurmoo, B. Moubaraki, K. S. Murray and D. J. Price, *J. Chem. Soc., Dalton Trans.*, 1999, 2987-2997.

2. G. J. Halder, C. J. Kepert, B. Moubaraki, K. S. Murray and J. D. Cashion, *Science*, 2002, **298**, 1762-1765.

3. M. Kurmoo, *Chem. Soc. Rev.*, 2009, **38**, 1353-1379.

4. S.-K. Yoo, J. Y. Ryu, J. Y. Lee, C. Kim, S.-J. Kim and Y. Kim, *J. Chem. Soc., Dalton Trans.*, 2003, 1454-1456.

5. S. Biswas, M. Maes, A. Dhakshinamoorthy, M. Feyand, D. E. De Vos, H. Garcia and N. Stock, *J. Mater. Chem.*, 2012, **22**, 10200-10209.

6. F. X. Llabres i Xamena, F. G. Cirujano and A. Corma, *Micropor. Mesopor. Mater.*, 2012, **157**, 112-117.

7. D. N. Dybtsev, H. Chun, S. H. Yoon, D. Kim and K. Kim, *J. Am. Chem. Soc.*, 2004, **126**, 32-33.

8. K. Uemura, S. Kitagawa, M. Kondo, K. Fukui, R. Kitaura, H.-C. Chang and T. Mitzutani, *Chem. Eur. J.*, 2002, **8**, 3586-3600.

9. M. Maes, F. Vermoortele, L. Alaerts, J. F. M. Denayer and D. E. De Vos, *J. Phys. Chem. C*, 2011, **115**, 1051-1055.

10. M. Kondo, T. Yoshitomi, K. Seki, H. Matsuzaka and S. Kitagawa, *Angew. Chem., Int. Ed. Engl.*, 1997, **36**, 1725-1727.

11. P. Losier and M. J. Zaworotko, *Angew. Chem., Int. Ed. Engl.*, 1996, **35**, 2779-2782.

12. H. Gudbjartson, K. Biradha, K. M. Poirier and M. J. Zaworotko, *J. Am. Chem. Soc.*, 1999, **121**, 2599-2600.

13. M. J. Hannon, C. L. Painting, E. A. Plummer, L. J. Childs and N. W. Alcock, *Chem. Eur. J.*, 2002, **8**, 2225-2238.

14. S.-i. Noro, R. Kitaura, M. Kondo, S. Kitagawa, T. Ishii, H. Matsuzaka and M. Yamashita, *J. Am. Chem. Soc.*, 2002, **124**, 2568-2583.

15. Y. Kim and D. Y. Jung, *Chem. Commun.*, 2002, 908-909.

16. M. Du, X.-H. Bu, Y.-M. Guo, J. Ribas and C. Diaz, *Chem. Commun.*, 2002, 2550-2551.

17. M. Haouas, C. Volkringer, T. Loiseau, G. Feréy and F. Taulelle, *Chem. Mater.*, 2012, **24**, 2462-2471.

18. J. A. Rood, W. C. Boggess, B. C. Noll and K. W. Henderson, *J. Am. Chem. Soc.*, 2007, **129**, 13675-13682.

19. I. H. Lim, W. Schrader and F. Schueth, *Chem. Mater.*, 2015, **27**, 3088-3095.

20. S. Surblé, F. Millange, C. Serre, G. Feréy and R. I. Walton, *Chem. Commun.*, 2006, 1518-1520.

21. M. Shoaee, M. W. Anderson and M. P. Attfield, *Angew. Chem., Int. Ed. Engl.*, 2008, **47**, 8525-8528.

22. P. Cubillas, M. W. Anderson and M. P. Attfield, *Chem. Eur. J.*, 2012, **18**, 15406-15415.

23. O. Shekhah, H. Wang, D. Zacher, R. A. Fischer and C. Wöll, *Angew. Chem., Int. Ed. Engl.*, 2009, **48**, 5038-5041.

24. Y. Chen, J. Zhang, J. Li and J. V. Lockard, *J. Phys. Chem. C*, 2013, **117**, 20068-20077.

25. H. C. Garcia, R. Diniz, M. I. Yoshida and L. F. C. de Oliveira, *J. Molec. Struct.*, 2010, **978**, 79-85.

26. N. Nijem, P. Thissen, Y. Yao, R. C. Longo, K. Roodenko, H. Wu, Y. Zhao, K. Cho, J. Li, D. C. Langreth and Y. J. Chabal, *J. Am. Chem. Soc.*, 2011, **133**, 12849-12857.

27.   M.-H. Zeng, Z. Yin, Y.-X. Tan, W.-X. Zhang, Y.-P. He and M. Kurmoo, *J. Am. Chem. Soc.*, 2014, **136**, 4680-4688.

28.   D. Y. Siberio-Perez, A. G. Wong-Foy, O. M. Yaghi and A. J. Matzger, *Chem. Mater.*, 2007, **19**, 3681-3685.

29.   D. Jiang, A. Urakawa, M. Yulikov, T. Mallat, G. Jeshke and A. Baiker, *Chem. Eur. J.*, 2009, **15**, 12255-12262.

30.   K. Mauger-Sonnek, L. K. Streicher, O. P. Lamp, A. Ellern and C. L. Weeks, *Inorg. Chim. Acta*, 2014, **418**, 73-83.

31.   K. Biradha, Y. Hongo and M. Fujita, *Angew. Chem., Int. Ed. Engl.*, 2000, **39**, 3843-3845.

32.   J. Bevitt, PhD Thesis, The University of Sydney, 2006.

33.   X. Zhao, R. Chen, C. Tengroth and T. G. Spiro, *Appl. Spectrosc.*, 1999, **53**, 1200-1205.

34.   A. Topaçli and S. Akyüz, *Spectrochim. Acta*, 1995, **51A**, 633-641.

35.   H. C. Garcia, R. Diniz, M. I. Yoshida and L. F. C. de Oliveira, *J. Molec. Struct.*, 2010, **978**, 79-85.

36.   D. S. Caswell and T. G. Spiro, *Inorg. Chem. Commun.*, 1987, **26**, 18-22.

37.   R. V. Biagetti and H. M. Haendler, *Inorg. Chem.*, 1966, **5**, 383-386.